

Supporting information for

**Flexoelectric Enhanced Film for Ultrahigh Tunable
Piezoelectric-like Effect**

Hui Ji ^{a#}, Shuwen Zhang ^{a#*}, Kaiyuan Liu ^a, Tonghui Wu ^a, Shuaijun Li ^{b,c}, Hao Shen ^d, Minglong Xu ^{a*}

^a State Key Laboratory for Strength and Vibration of Mechanical Structures, School of Aerospace Engineering, Xi'an Jiaotong University, Xi'an 710049, China

^b Department of Biophysics, School of Basic Medical Sciences, Key Laboratory of Environment and Genes Related to Diseases, Health Science Center, Xi'an Jiaotong University, Xi'an, 710061, China

^c Department of Oncology, The Second Affiliated Hospital, Medical School of Xi'an Jiaotong University, Xi'an, 710061, China

^d Center for Advancing Materials Performance from the Nanoscale (CAMP-Nano), State Key Laboratory for Mechanical Behavior of Materials, Xi'an Jiaotong University, Xi'an, Shaanxi 710049, China

Corresponding authors' email: zhang.shuwen@xjtu.edu.cn, mlxu@xjtu.edu.cn

These authors contributed equally to this work.

Mechanism of enhanced Flexoelectricity in FEEF

A 3D elastomeric network with immobilized NPs can be simplified as a 2D neighboring network structure (Figure S1A). Electric polarization defines the accumulation of separated charges at the interfaces between a dielectric and two electrodes. As shown in Figure S1B(I), in the crosslinked polymer networks, the centers of positive and negative charges coincide initially when there is no asymmetric deformation. When a cubic network of elastomer is subjected to a bending motion, a curvature k occurs on horizontal direction, each bended network generates electric dipole moment $p = qd$, where q and d are the equivalent electric charges per network and the separating distance between positive and negative charges due to bending, respectively. Therefore, the flexoelectric polarization P is the total electric dipole moments per unit volume, which can be described as

$$P = \frac{\sum p}{V} = \mu_0 k, \quad (\text{S1})$$

where V and μ_0 are the total volume of the unit cell and initial flexoelectric coefficient of the elastomer. As the relationship between flexoelectric coefficient μ and uniaxial pre-stretch λ is $\mu \sim \lambda^{2[1,2]}$. When the biaxial pre-stretch is applied on the elastomer, the flexoelectric coefficient can be enhanced as

$$\mu_0 \sim \lambda_x^2 + \lambda_y^2, \quad (\text{S2})$$

where λ_x and λ_y are the biaxial pre-stretch ratios along x and y direction, respectively.

When NPs are introduced into elastomer matrices, the cubic unit cells immobilized with NPs are enlarged with longer chains (Figure S1B(II)). The enlarged meshes generate initial strain gradient k_0 with neighboring meshes, each of which leads to an initial dipole moment of qd_0 , where d_0 is the initial distance of positive and negative charges. If the NP is electrically charged (Figure S1B(III)), the initial dipole moment will be

$$p_0 = (q + q_e)d_0, \quad (\text{S3})$$

where q_e is the increment of equivalent electric charge in a polymer network by charged NP. Before bending, the initial dipole moments cancel each other out. When subjecting a curvature k to the structure, it can be assumed that a dipole moment of p is applied on each of the neighboring meshes. The total polarization can be calculated as

$$P_1 = \frac{\sum [p + (2p + 4p_0 \sin ak)w]}{V} = (1 + 2w)\mu_0 k + \frac{4w \sin ak \sum p_0}{V}, \quad (\text{S4})$$

Where w and a are the weight ratio of the filled NPs and the length of the polymer chain in unit cell, respectively. Therefore, the effective flexoelectric coefficient μ_1 can be described as

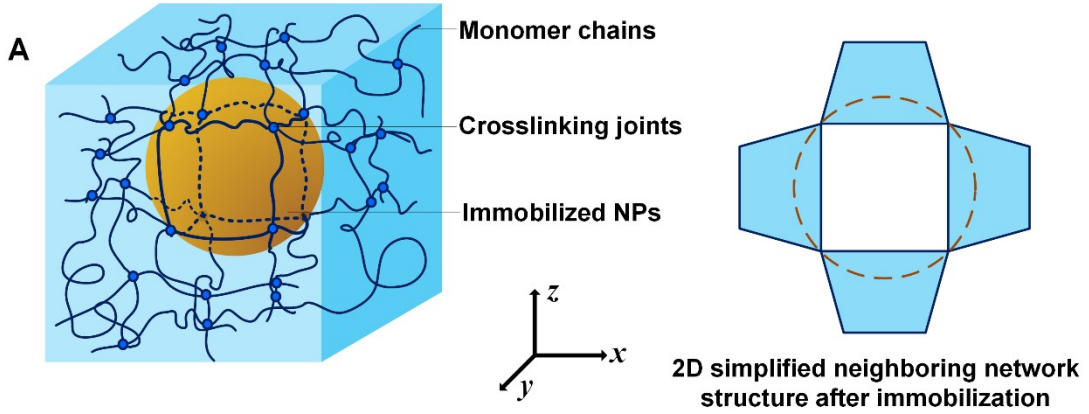
$$\mu_1 = \frac{P_1}{k} = (2w+1)\mu_0 + \frac{4w \sin ak \sum (q_e + q_e) d_0}{Vk} \approx (2w+1)\mu_0 + \frac{4w \sin ak \mu_0 k_0 (1 + \frac{q_e}{q})}{k}. \quad (\text{S5})$$

Since $a \sim 10^{-9}$ m, $ak \sim 0$, then $\sin ak \approx ak$. Eq. (S5) can be simplified as

$$\mu_1 \sim [4wak_0(1 + \frac{q_e}{q}) + 2w+1]\mu_0. \quad (\text{S6})$$

Considering the effect of biaxial pre-stretch, the flexoelectric effect of FEEF can be described as

$$\mu_1 \sim [4wak_0(1 + \frac{q_e}{q}) + 2w+1](\lambda_x^2 + \lambda_y^2)\mu_0. \quad (\text{S7})$$



B

	Initial	Bending	Pre-stretch & bending
I	 $p_I = 0$	 $p_I = \sum p$	 $p_I = (\lambda_x^2 + \lambda_y^2) \sum p$
II	 $p_{II} = 0$	 $p_{II} = 0$	 $p_{II} = 0$
III	 $p_{III} = 0$	 $p_{III} = 0$	 $p_{III} = 0$

Figure S1. (A) 3D and 2D schemes of elastomer matrices with immobilized NPs. (B) Electromechanical analysis for (I) pure elastomer, (II) elastomer with immobilized NPs, (III) elastomer with electrically charged NPs under initial, bending and pre-stretch conditions.

Strain gradient in transverse flexoelectricity

There are two traditional setups to study transverse flexoelectricity (Figure S2). When a beam is bent in three-point-bending motion, the average strain gradient along thickness direction z can be derived from normal equations as^[3]

$$\frac{\partial \varepsilon_{xx}}{\partial z}_{\text{average}} = 3z_0 \left(\frac{L}{2}\right)^{-3} \left(\frac{L}{2} - x_1\right), \quad (\text{S8})$$

where z_0 is the displacement at the middle of the beam, L is the length of the beam between two supporting bars, and x_1 is the distance to the middle of the beam (Figure S2(A)). When a membrane with fixed lateral boundary is bent by applying point load in the center, according to theories of plates and shells^[4], the differential equation of bending a circular plate can be written as

$$D\nabla_r^2 \nabla_r^2 w = q(r, \theta), \quad (\text{S9})$$

where D , w , q , r and θ are the bending rigidity, deflection, load distribution, radius direction and peripheral direction of cylinder coordinate system. And

$$\left\{ \begin{array}{l} \nabla_r^2 = \frac{\partial^2}{\partial r^2} + \frac{1}{r} \frac{\partial}{\partial r} + \frac{1}{r^2} \frac{\partial^2}{\partial \theta^2} \\ D = \frac{Eh^3}{12(1-\nu^2)} \end{array} \right., \quad (\text{S10})$$

with Poisson's ratio ν . In the case of axial symmetry, Eq. (S9) can be written as

$$\left(\frac{d^2}{dr^2} + \frac{1}{r} \frac{d}{dr}\right) \left(\frac{d^2 w}{dr^2} + \frac{1}{r} \frac{dw}{dr}\right) = \frac{q(r)}{D}. \quad (\text{S11})$$

And the bending moment along radius and peripheral direction (M_r and M_θ) can be calculated as

$$\left\{ \begin{array}{l} M_r = -D \left(\frac{d^2 w}{dr^2} + \frac{\nu}{r} \frac{dw}{dr} \right) \\ M_\theta = -D \left(\nu \frac{d^2 w}{dr^2} + \frac{1}{r} \frac{dw}{dr} \right) \end{array} \right. \quad (\text{S12})$$

Considering the boundary conditions of this case,

$$q(0) = P, \quad w(a) = 0, \quad \frac{\partial w(a)}{\partial r} = 0, \quad (\text{S13})$$

where P is the applied force in the center of the circular plate and a is the radius of the plate. The deflection of the plate can be expressed as

$$w = \frac{P}{16\pi D} \left(2r^2 \ln \frac{r}{a} + a^2 - r^2 \right). \quad (\text{S14})$$

The largest deflection w_0 , which obviously occurs in the center of the plate ($r = 0$), is

$$w_0 = w(0) = \frac{Pa^2}{16\pi D}. \quad (\text{S15})$$

Then Eq. (S12) can be simplified as

$$\begin{cases} M_r = \frac{P}{4\pi} \left[(1+\nu) \ln \frac{a}{r} - 1 \right] \\ M_\theta = \frac{P}{4\pi} \left[(1+\nu) \ln \frac{a}{r} - \nu \right] \end{cases}. \quad (\text{S16})$$

Normal stress σ_r and σ_θ can be calculated as

$$\begin{cases} \sigma_r = \frac{3Pz}{\pi h^3} \left[(1+\nu) \ln \frac{a}{r} - 1 \right] \\ \sigma_\theta = \frac{3Pz}{\pi h^3} \left[(1+\nu) \ln \frac{a}{r} - \nu \right] \end{cases}. \quad (\text{S17})$$

Then normal strain ε_r and ε_θ are

$$\begin{cases} \varepsilon_r = \frac{\sigma_r}{E} = \frac{4w_0z}{a^2(1-\nu^2)} \left[(1+\nu) \ln \frac{a}{r} - 1 \right] \\ \varepsilon_\theta = \frac{\sigma_\theta}{E} = \frac{4w_0z}{a^2(1-\nu^2)} \left[(1+\nu) \ln \frac{a}{r} - \nu \right] \end{cases}. \quad (\text{S18})$$

Since the circular plate is axial symmetry, the strain along peripheral direction is neglected. Then we have transverse strain gradient as

$$\frac{\partial \varepsilon_r}{\partial z} = \frac{4w_0}{a^2(1-\nu^2)} \left[(1+\nu) \ln \frac{a}{r} - 1 \right]. \quad (\text{S19})$$

In this case, we calculated the average strain gradient as

$$\frac{\partial \varepsilon_r}{\partial z}_{\text{average}} = \frac{\int_{r_1}^{r_2} \frac{4w_0}{a^2(1-\nu^2)} \left[(1+\nu) \ln \frac{a}{r} - 1 \right] dr}{r_2 - r_1}. \quad (\text{S20})$$

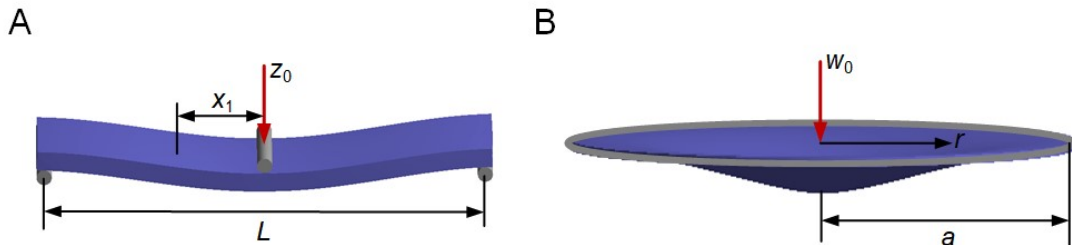


Figure. S2. Setups for the study of transverse flexoelectricity: bending motion of (A) beam with three-point supporting and (B) membrane with fixed lateral boundary.

Finite element Analysis (FEA) by ANSYS Workbench is carried out to verified the

strain gradient distribution. For circular membrane, the detail setup is listed in Table S1. Static analysis is considered as the experimental frequency is below 10 Hz. Concentrated load in the center of the membrane is controlled by the displacement at the center of the membrane, which is 0.1 mm in this FEA simulation. The elastic modulus and Poisson's ratio are set as 2.0 MPa and 0.49. Strain distribution on bottom and upper layers of circular membrane are shown in Fig. S3(A), revealing the opposite sign of strain gradient along radius direction. In order to avoid the impact by stress concentration in the center and neutralization of strain gradient with opposite sign, the flexoelectric measurements is optimized by setting electrode on specific areas. Fig. 3(B) shows the strain gradient comparison between FEA result and theoretical calculation. The average strain gradient by FEA and theory are -0.66 and -0.63 respectively in the region of $10 \text{ mm} < r < 18 \text{ mm}$. With an acceptable error of 4.55 %, electrodes are determined in the region of $10 \text{ mm} < r < 18 \text{ mm}$ as shown in Fig. S3(B). For three-point bending beam, we just use Eq. (S8) to calculate the strain gradient, since it's a regular method to study transverse flexoelectricity^[3,5,6].

Table S1. FEA setup for bending a circular membrane

Geometry	Radius/mm	Thickness/mm	Constraint	Load	Material
Circular membrane	20	0.6	Fixed lateral constraint	Concentrated load in the center	PDMS

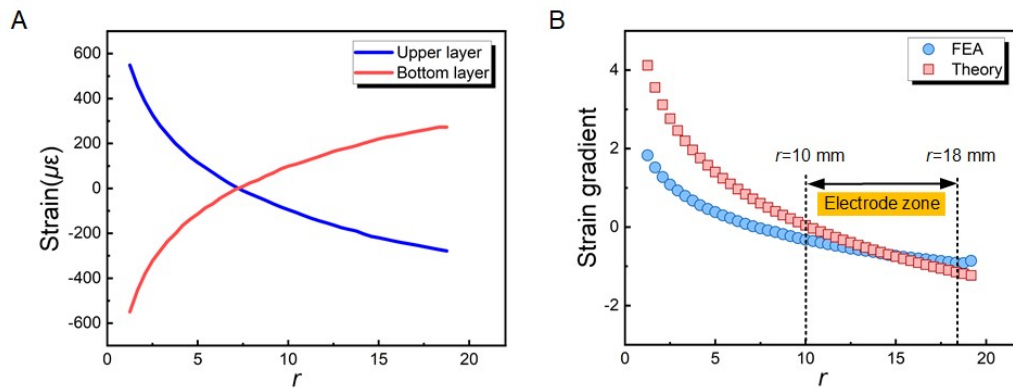


Figure. S3 (A) Strain distribution of upper and bottom layers through FEA simulation along radius direction for circular membrane. (B) Strain gradient comparison between FEA and theoretical calculation.

Material preparation

Polydimethylsiloxane (PDMS) is used as a typical elastomer in this work. The experimental samples are made by commercial SYLGARD 184 silicone elastomer^[7]. PDMS precursor are mixed at certain weight ratios of SYLGARD 184 base and curing agent, while corresponding mesh sizes are calculated (Table S2)^[1]. NPs are mixed into

ethanol. Then we put PDMS precursor together with NP-ethanol liquid. The mixture is stirred and poured into an aluminum mould. After heating at 60 °C for 24 hours, the PDMS-NP composite is solidified. For electric poling, we borrow the aluminum mould as negative electrode and cover another metal plate as positive electrode on the upper surface of the sample. A heat plate (MS7-H550-Pro, DLAB) under the aluminum mould is used to keep a constant elevated temperature during poling process. In the thermal poling process, the sample is heated from room temperature to 150 °C. After maintaining 150 °C for 20 minutes, the heat plate is switched off and cools down until room temperature. During the whole process, the sample is applied with an electric field by a high voltage source. After poling, the sample is cut into designed shape for further biaxial pre-stretch and flexoelectric measurement. Stretchable carbon conductive grease (#846-80G, MG Chemicals) is adopted as electrode, which are coated in certain area defined by Figure. S3(B).

Table S2

Curing ratio	10:1	12:1	15:1	18:1	20:1
Measured modulus (MPa)	2.804	2.162	1.896	1.601	1.007
Calculated Mesh size (nm)	1.64	1.79	1.87	1.98	2.30

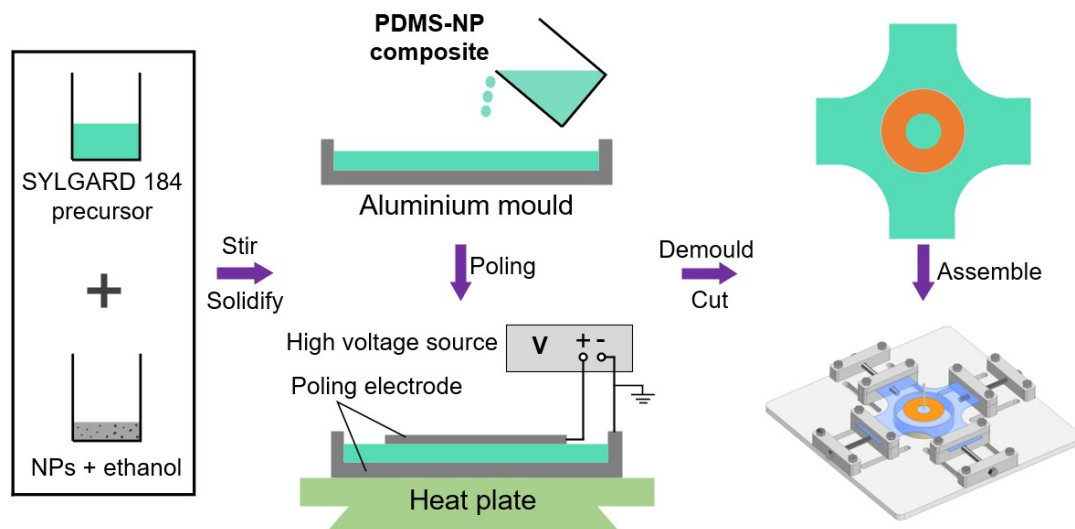


Figure. S4. Material preparation procedure.

Experiment measurement for transverse flexoelectricity

The experimental setup of bending a circular FEEF membrane is shown in Figure S4a. Sinusoidal loads with a frequency of 1 Hz were applied on the samples to generate a displacement load using a material load machine MTS-858. The induced flexoelectric electric polarizations were detected by a charge amplifier B&K2692A by connecting both wires to the electrodes on both surfaces of the membrane. Displacement load and

voltage signals were displayed in real time and recorded by a Tektronix MDO3104 oscilloscope. Pure PDMS, PDMS-NP composite and poled PDMS-NP composite are prepared in the experiments. All three types of samples are tested with different biaxial pre-stretch ratios. Five incremental displacement loads are set, while strain gradients are calculated according to Eq. (S20) (Table S3). With the measured electric charges divided by the area of electrode, polarization is obtained. According to Eq. (1), Flexoelectric coefficients are calculated and listed in Table S4 partially.

Table S3

Displacement (mm)	0.1	0.2	0.3	0.4	0.5
Strain gradient (m ⁻¹)	0.63	1.26	1.89	2.52	3.05

Table S4

μ_{flexo} (nC/m)	Biaxial pre-stretch				
	1.0×1.0	1.1×1.1	1.2×1.2	1.3×1.3	1.4×1.4
Pure PDMS	0.086	0.12	0.23	0.45	0.64
PDMS-NP	0.333	1.04	1.75	2.35	3.72
Poled PDMS-NP	1.01	2.24	4.75	5.67	7.46

Three-point-bending experiment validation

We also perform three-point beam bending experiment to verify the proposed three-dimensional (3D) membrane bending approach (Figure S2(A), S5(B)). With a similar experimental method, we measured the flexoelectric coefficients of pure PDMS under biaxial pre-stretch (Table S5). The results of three point bending method are comparable to 3D membrane bending. The discrepancy is mainly due to the nonuniform strain gradient distribution.

Table S5

$\square \mu_{\text{flexo}}$ (nC/m)	λ_y			
	1.0	1.1	1.2	
λ_x	1.0	0.126	0.174	0.249
	1.1	0.178	0.240	0.210
	1.2	0.180	0.274	0.326

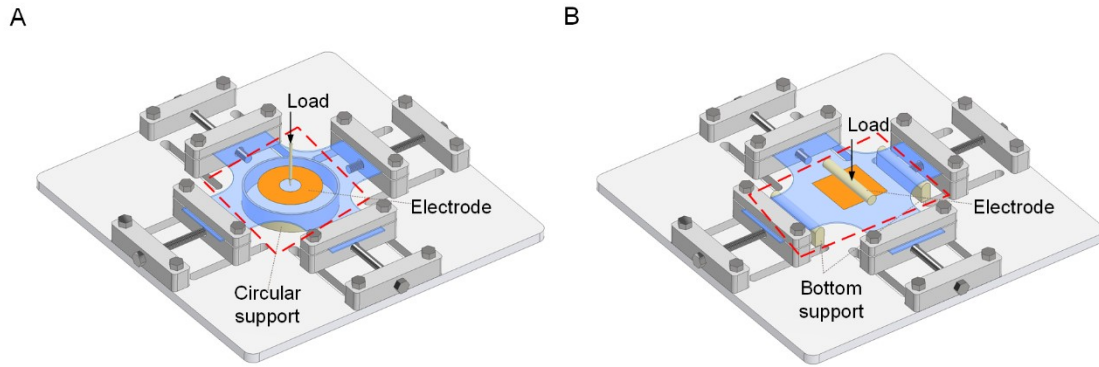


Figure. S5 Experimental setups. (A) Bending a circular membrane under pre-stretch, (B) Three-point beam bending under pre-stretch.

Nano particle Selection

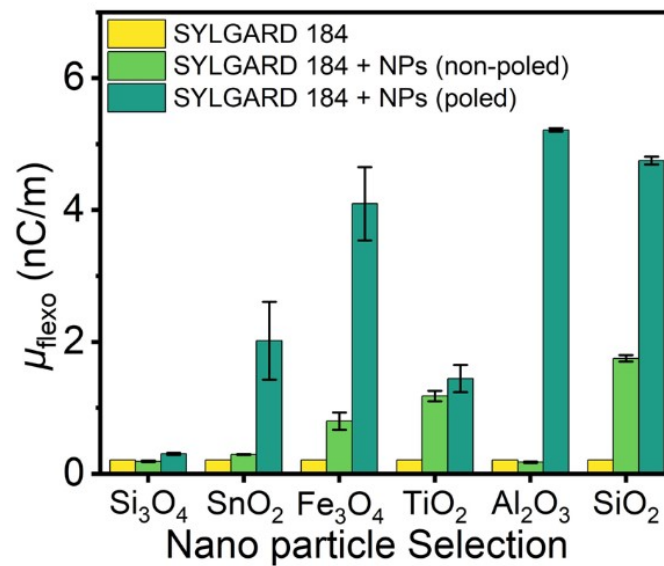


Figure. S6 NP selection. Flexoelectric coefficients of biaxial pre-stretched SYLGARD 184-NP composite with different type of NPs. It is seen from (G) that silica, Al₂O₃, and Fe₃O₄ NP fillings could extensively enlarge the flexoelectric coefficients.

Mechanical design of FEEF

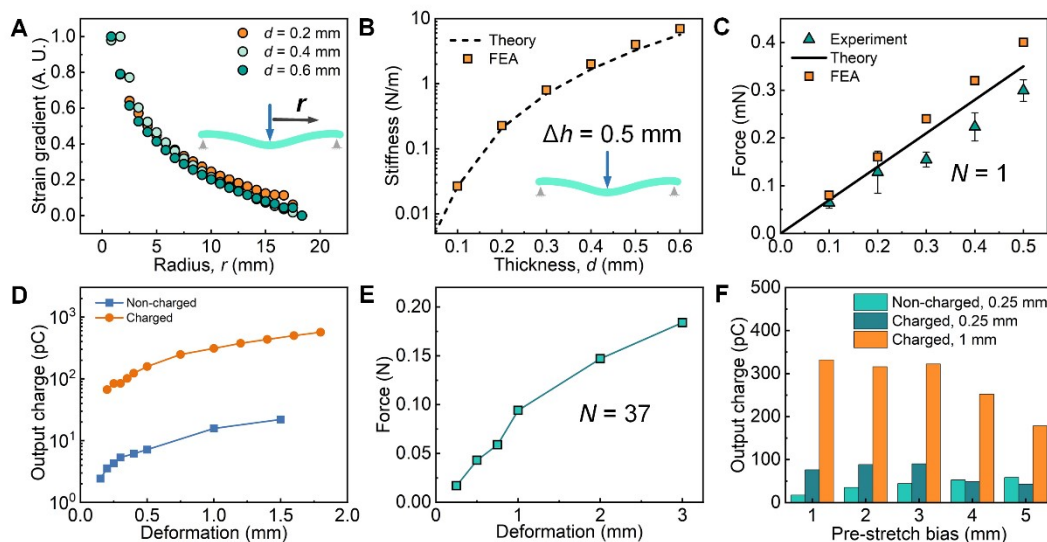


Figure. S7 Mechanical properties of FEEF. **(A)** Strain gradient distribution of poking a circular film through FEA. **(B)** Equivalent stiffness of a circular film in bending motion regarding to thickness t . **(C)** Force-deformation relationship in poking a circular film. **(D)** Electro-mechanical performance, **(E)** measured load with respect to deformation under multiple poking actuators ($N = 37$). **(F)** Electro-mechanical response with respect to pre-stretch bias.

Size characterization of silica NPs

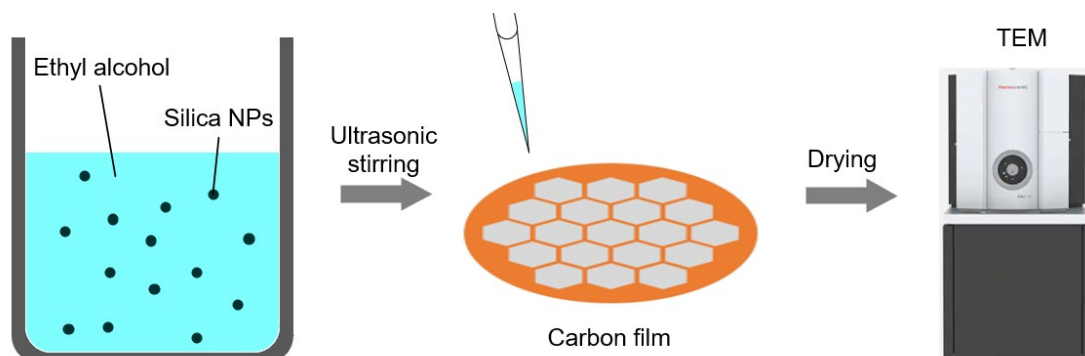


Figure S8 TEM measurement procedures. The actual sizes of silica NPs are experimentally measured by Transmission Electron Microscope (Talos L120C TEM, Thermo Fisher Scientific). The silica NPs are mixed with ethyl alcohol (2 mg/mL). The mixture is stirred by ultrasonic mixer for 2 hours to separate the NPs. Then the mixed liquid is dripped onto a carbon film. After 12 hours until the ethyl alcohol volatilizes thoroughly, the carbon film with silica NPs is ready to use in the TEM.

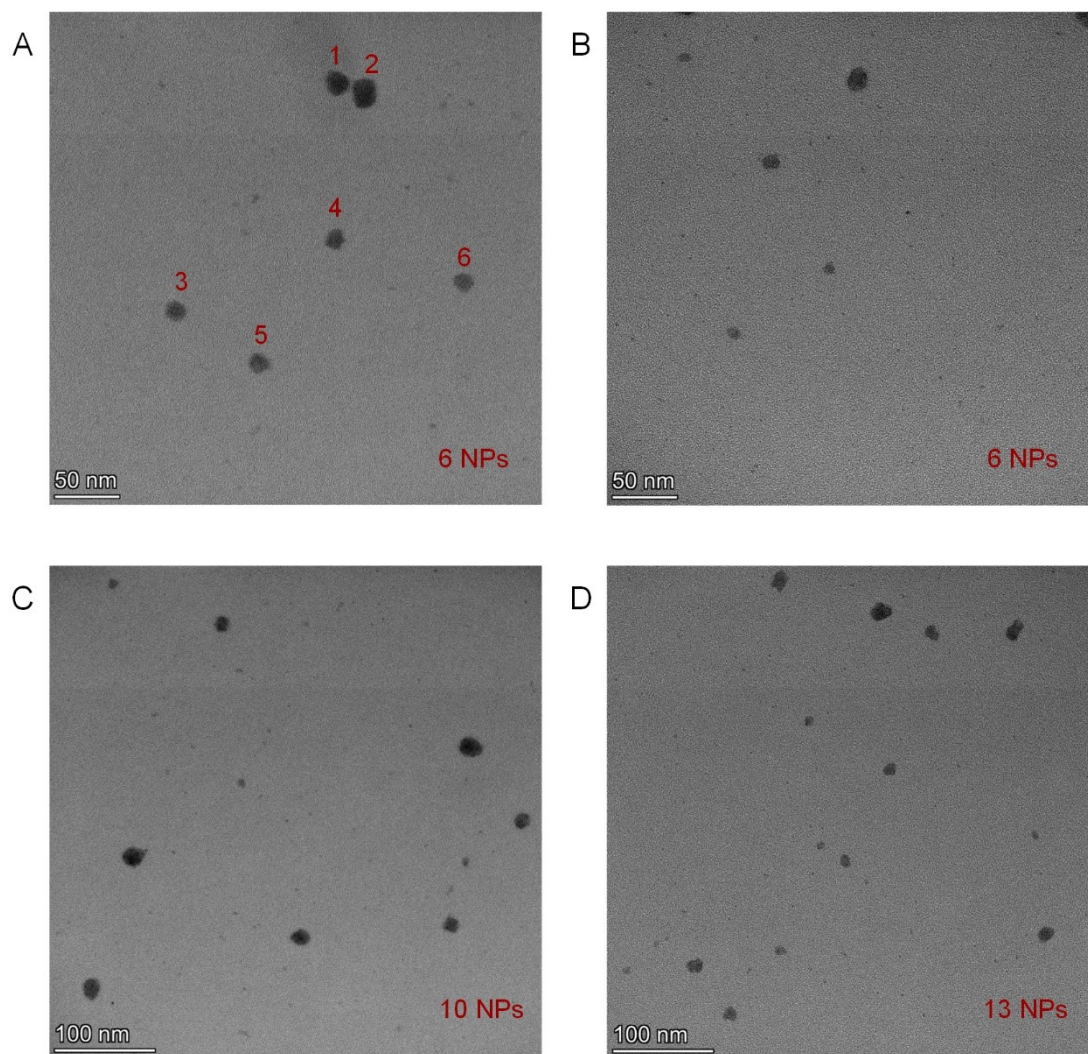


Figure S9 TEM images with numbers of displayed spherical silica NPs with scale bar of 50 nm and 100 nm, (A) 6 NPs, (B) 6 NPs, (C) 10 NPs and (D) 13 NPs.

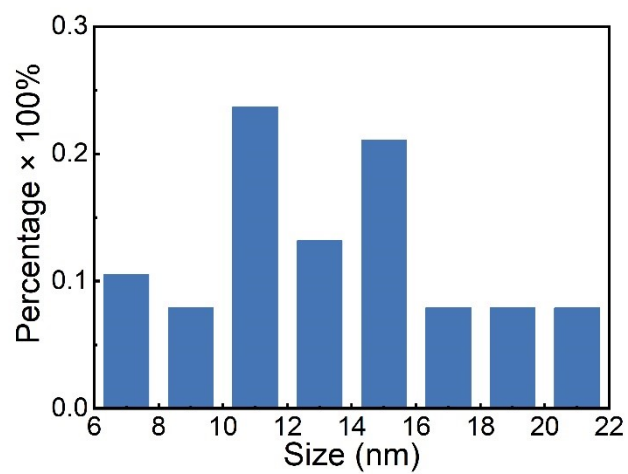


Figure S10 Statistical size distribution silica NPs. The total number of silica NPs is 35 counted in Figure S9. The actual diameters of these spherical silica NPs are distributed within 6 nm to 20 nm,

and the average diameter is calculated as 12.9 nm.

Mechanical properties of the film with respect to silica weight ratios

we have investigated the mechanical properties of the composite with different weight ratio (from $w = 0.0\%$ to 0.7%) at uniaxial tension (Figure S11A). With $w < 0.4\%$, the tensile stress of the composite keeps constant, while the tensile stress increases when $w > 0.4\%$ (Figure S11B). The maximum stretching ratio of the composite before fracture with respect to silica weight ratio is shown in Figure S11C. When $w < 0.4\%$, the maximum stretching ratio of the composite remains stable with average value of 2.4. When $w > 0.4\%$, the maximum stretching ratio of the composite decreases with respect to silica weight ratio. Experiments show that the PDMS-NP composite with silica weight ratio more than 0.4% becomes stiffer and the stretchability decreases, which means it needs more mechanical load to deform and has smaller deformability.

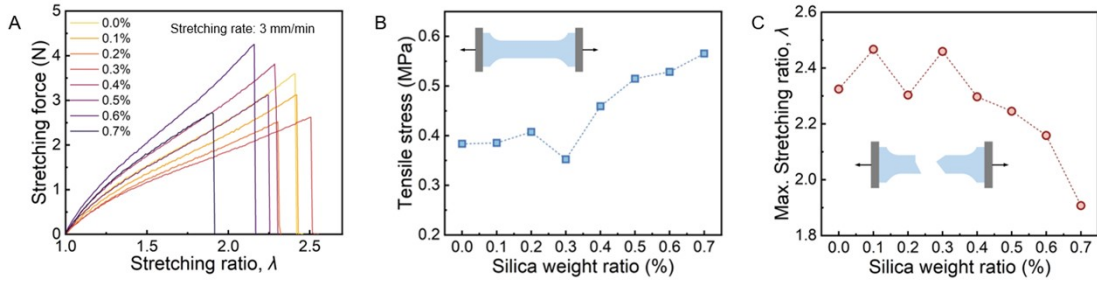


Figure S11 Mechanical properties of PDMS-NP composite. (A) Stress-stretch curves under uniaxial tension. (B) The tensile stress of the composite with silica NPs weight ratio from 0.0% to 0.4% keeps at a level of around 0.4 MPa, while when the silica weight ratio more than 0.4%, the tensile stress of the composite increase rapidly. (C) Maximum stretching ratio of the composite with silica weight ratio less than 0.4% is around 2.4, while when the silica weight ratio more than 0.4%, maximum stretching ratio drops with respect silica weight ratio.

Electrical charging of the film

We have explained the effect of the electric charging by characterizing the surface charge density of the film by two different ways.

a) By surface potential

The electrical charging procedure has key impact on the electromechanical property of the composite. Upon charging, net charges are trapped by the material. The net charge level can be reflected by the surface charge density D_s of the material. We have measured the surface charge density D_s of the composite with different silica weight ratios after electrical charging. The un-charged and charged D_s are experimented by an indirect way of measuring the surface potential V_s . Then the surface charge density D_s can be predicted by the following equation (*Appl. Phys. Lett.* 1975, 26(12), 675-677):

$$D_s = \frac{\varepsilon_r \varepsilon_0 V_s}{t}, \quad (\text{S21})$$

where ε_r and t represent the permittivity and thickness of the composite, respectively. The relative permittivity of the composite with different silica weight ratio is indirectly obtained by measuring the capacitance C , and calculated by

$$\varepsilon_r = \frac{Ct}{\varepsilon_0 A}, \quad (\text{S22})$$

where A is the area of the measuring surface. The capacitance is measured by an LCR meter (HIOKI, IM 3533-01). The surface potential is measured by an electrostatic meter (Trek MODEL P0865). Then we have the surface charge density D_s with respect to silica weight ratios w as shown in Figure 2D(iii) in the revised manuscript. Similar experiment results can be found in previous work (*NANO LETT.* 2020, 20, 4580-487). Results show that D_s increases with the amount of silica when $w \leq 0.2\%$. When $w > 0.2\%$, D_s stays steady. The observed ‘‘plateau charge density’’ is understood as follows.

The electrical breakdown strength of PDMS is much larger than that of air. Consequently, when the composite is electrically charged and the top electrode is then removed, the surface charge density of the composite is thus limited by the breakdown of air. Given the electric breakdown strength of air, $E_B \sim 10^6 \text{ V m}^{-1}$ and the permittivity, $\varepsilon \sim 10^{-11} \text{ F m}^{-1}$, the upper limit of the surface charge density of the composite, $q \sim \varepsilon E_B \sim 10^{-5} \text{ C m}^{-2}$. This order of magnitude is consistent with the experimentally observed upper bound. Therefore, the composite with silica weight ratio of 0.2% have already reach a high level of surface charge density after electrical charging. Larger amount of silica NPs has little impact on enhancing the electromechanical property of the composite.

b) By comparing displacement of the film in electric field

In Figure 2D(ii), the film with surface charge density in an electric field will be bent by the force of electric field. When subjected to an electric field by applying opposite voltages on both electrodes, the boundary condition of the film with negative surface charge density D_s can be simplified as a cantilever beam with uniformly distributed load p . The relationship between p and applied voltage V can be described as

$$p = \frac{D_s b V}{(h+t)}, \quad (\text{S23})$$

where $h/2$ is the distance between the electrode and the film, t and b are the thickness

and width of the film. The maximum displacement of the cantilever v_{\max} at the free end is

$$v_{\max} = \frac{-pl^4}{8EI} = \frac{-3D_sVL^4}{2E(h+t)t^3}, \quad (\text{S24})$$

where L and E are the length and elastic modulus of the beam, $I = bt^3/12$ is the bending stiffness of the beam, respectively. The v_{\max} in Figure 2D(ii) is measured as 8 mm for the charged film and 2.5 mm for the non-charged film. The other parameters are listed as : $t = 0.6$ mm, $h = 30$ mm, $b = 15$ mm, $l = 55$ mm, $E = 2.8$ MPa and $V = 600$ V. According to Eq. (S24), the surface charge density can be calculated as $17.6 \mu\text{C}/\text{m}^2$ for the charge film and $5.5 \mu\text{C}/\text{m}^2$ for the non-charged film. The surface charge density of the charged and non-charged film is in good agreement with the results in Figure 2D(iii). The deviation is mainly from the inaccurate measurement and the simplification of the cantilever beam model.

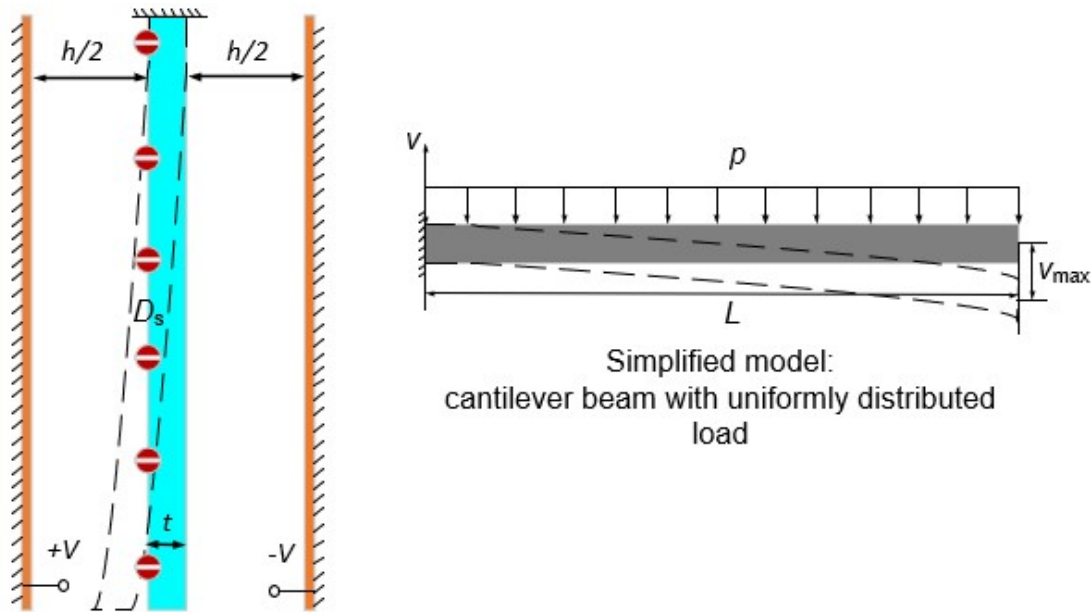


Figure S12 Theoretical model of charged film in an electric field.

References

- [1] S. Zhang, K. Liu, T. Wu, M. Xu, S. Shen, *J. Phys. Chem. C* **2020**, *124*, 24429.
- [2] H. Ji, S. Shao, K. Liu, H. Shang, Y. Zhu, T. Wu, S. Shen, S. Zhang, M. Xu, *Applied Physics Letters* **2021**, *6*.
- [3] P. Zubko, G. Catalan, A. Buckley, P. R. L. Welche, J. F. Scott, *Phys. Rev. Lett.* **2007**, *99*, 167601.
- [4] H. Fubao, S. Yapeng, *Xi'an Jiaotong University* **1993**.
- [5] S. Zhang, M. Xu, G. Ma, X. Liang, S. Shen, *Jpn. J. Appl. Phys.* **2016**, *55*, 071601.
- [6] X. Wen, G. Yang, Q. Ma, Y. Tian, X. Liu, D. Xue, Q. Deng, S. Shen, *Journal of Applied Physics* **2021**, *130*, 074102.

[7] T. D. C. Company, **2017**, 4.